Aspherical laser resonators: An analogy with quantum mechanics

C. Paré,* L. Gagnon, and P. A. Bélanger
Equipe Laser et Optique Guidée, (COPL) Département de Physique, Université Laval, Sainte-Foy, Québec, Canada G1K 7P4
(Received 1 May 1992)

We develop an analogy between the transverse modes of a class of aspherical laser resonators and the eigenstates of the stationary Schrödinger equation with a potential well directly related to the mirror profile. Using a perturbation method, the equivalence is shown to be valid for a short cavity length in comparison with the Rayleigh range of the fundamental mode, i.e., the most practical situation. Numerical examples with mirror profiles corresponding to a Pöschl-Teller potential confirm the validity of the model. The analysis also includes higher-order corrections for the case of a longer resonator length. The analogy with quantum mechanics should be useful for designing laser resonators with a high discrimination against higher-order transverse modes.

PACS number(s): 42.60.Da, 03.65.Ge, 42.25.−p, 03.40.Kf

I. INTRODUCTION

Optical laser resonators generally consist of open cavities formed with two spherical mirrors enclosing gain and modulation elements. The analysis of the spherical resonator is now standard [1–3] and leads to a classification of the resonators as "stable" or "unstable" cavities. To be of good quality, a laser beam must oscillate in only one transverse mode which should cover a large fraction of the gain section of the amplifying medium. Owing to its geometrical magnification factor, the unstable resonator offers the advantage of providing a large mode volume as well as a high discrimination against the perturbing higher-order transverse modes. However, the magnification factor also implies an important geometrical loss for the fundamental mode. This is usually compensated for by using this loss as external coupling. Therefore, the unstable resonator is convenient for lasers with a very high gain in which case the high loss of the fundamental mode may correspond to the optimum coupling for an efficient operation [4].

On the other hand, lasers with medium or low gain are usually stable resonators with an optimized coupler reflectivity. The stable cavity has a low-loss confined mode but its beam size is rather small for typical experimental conditions where the stability against misalignment is always important. Moreover, this resonator presents a poor modal selectivity since the higher-order modes are also confined and nearly lossless.

In the past, workers have tried to combine the advantages of both types of resonator in the same cavity. Most of these efforts consisted in reducing the hard-edged diffraction of the unstable resonator by, for example, changing locally the mirror curvature near the edges or by introducing phase shifts near the edges or on the Fresnel zones [5]. Over the past few years, it has been widely recognized that the hard-edged diffraction in an unstable resonator can be best controlled by the use of a graded-reflectivity mirror (GRM) [6]. This confines the beam as in a stable cavity but the beam waist can be adjusted to the size of the gain medium. However, the feedback in a GRM unstable resonator is usually rather small and this technique is still mostly suitable to high-gain laser medium.

For the important class of medium- and low-gain lasers, a different solution for increasing the beam size still has to be demonstrated. If properly designed, the optical resonator formed with an *aspherical* mirror and a plane output coupler seems to us to be able to meet these specifications. In the past, only a few analyses (that we know of) of this type of resonator have been published [7–9]. The absence of exhaustive conclusions on the properties of aspherical resonators is largely due to the fact that such an investigation would imply numerical solution of coupled integral equations with a large number of parameters needed for specifying a sufficiently wide class of aspherical mirrors and the resonator dimensions. Along those lines, one must point out the work of Smithers and Ferguson [10] who introduced the idea of a locally varying magnification factor. Their analysis is based on geometrical optics and is applicable to unstable cavities, limiting the use again to high-gain laser systems.

More recently, we have proposed [11,12] a wide class of aspherical resonators which have the property of yielding a fundamental mode of prescribed shape and of the stable type. Our ultimate goal is a systematic specification of an aspherical resonator with (i) a predetermined fundamental mode of the stable type (low loss), and (ii) highly discriminated higher-order transverse modes. Our recent analysis of resonators with a super-Gaussian intensity output [11,12] indicates that this is possible for a broad band of resonator parameters; this has also been recently confirmed in the laboratory [13].

The analysis presented in this paper represents a further step toward this objective. In Sec. II, we first recall the main characteristics of this class of aspherical resonators and their design procedure. Then, using a perturbation method, we show that the confined transverse modes of a resonator of short cavity length obey a Schrödinger differential equation with a potential directly related to the mirror profile. This establishes a close relationship

between the confined modes of this resonator and the bound states of the corresponding potential. The analogy with quantum mechanics proves fruitful when we consider potential wells supporting only a limited number of bound states, which correspond to optical resonators having a limited number of confined modes. Here, we limit the analysis to the well-known Pöschl-Teller potential. The study of longer cavity resonators is also undertaken by including higher-order terms in the perturbation expansion.

In Sec. III, in order to assess the validity of our model, the modal properties of two different aspherical resonators are determined by solving the exact problem (integral equation) numerically. It is then shown that the reduction to a Schrödinger equation correctly predicts the main characteristics of these resonators. The higher-order corrections are also confirmed when a longer cavity is also considered. Finally, in conclusion, we return to the basic assumptions of the model and give an outline of its possible extensions and applications.

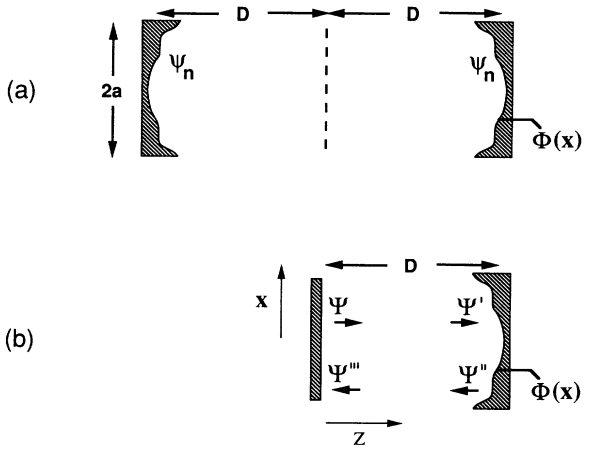

FIG. 1. (a) Schematic configuration of a symmetric aspherical resonator of length $L=2D$, with a mirror of radius a and phase profile $\Phi(X)$. ψ_n represents the modal distribution on the mirrors; (b) half-symmetric aspherical resonator of length D.

II. ANALYSIS

A. Statement of the problem

We consider the symmetric one-dimensional strip resonator depicted in Fig. 1(a) and formed with two identical graded-phase mirrors separated by a distance $L=2D$. (The extension to a cylindrical geometry is straightforward and will be discussed later in the Conclusion.) The phase profile $\Phi(X)$ of the mirror is, for now, unspecified. In the Huygens-Fresnel approximation, it can easily be shown that the transverse modes $\psi_n(X)$ of this symmetric optical cavity obey the following integral equation:

$$\left[\frac{i}{\lambda L}\right]^{1/2}\int_{-a}^{+a}\psi_n(X_1)\exp\left\{i\left[\Phi(X_1)+\Phi(X_2)-\frac{\pi}{\lambda L}(X_2-X_1)^2\right]\right\}dX_1=\gamma_n\psi_n(X_2)\ , \quad (2.1)$$

where ψ represents the field distribution on the mirrors of width $2a$, λ is the wavelength, and γ is the eigenvalue containing information on the diffraction loss and the axial phase shift.

Unfortunately, only the spherical mirror profiles $\Phi(X)$ (for which, in the paraxial approximation, $\Phi=kX^2/2R_M$, where $k=2\pi/\lambda$ and R_M is the radius of the mirror) allow an exact solution of Eq. (2.1). In that particular case, if one neglects hard-edged diffraction, i.e., in the limit $a\to\infty$, then the integral equation admits the set of Hermite-Gauss functions as exact solutions. For $g^2<1$, where $g=1-L/R_M$ is the so-called "geometric parameter," the wave front of these modes matches the surface of the mirror. The modes are then said to be "conjugated," in the sense that the reflected field is a phase-conjugate replica of the incoming distribution. This property implies the absence of geometrical loss ($|\gamma|=1$). Such a resonator is said to be stable. In contrast, the solutions of an unstable resonator ($g^2>1$) are uniform spherical waves that are not conjugated and then suffer an important geometrical loss ($|\gamma|<1$).

In this paper, we limit the analysis to the class of stable resonators, for which the transverse eigenmodes are conjugated in the limit $a\to\infty$. In the case where spherical mirrors are used, the width w_0 (at $1/e$ in amplitude) of the fundamental Gaussian mode at the center of the cavity is given by [14].

$$w_0=\left[\frac{1+g}{1-g}\right]^{1/4}w_{\text{conf}}\ , \quad (2.2)$$

where $w_{\text{conf}}=\sqrt{\lambda L/2\pi}$ is the width of the so-called "confocal resonator" ($g=0$, i.e., $R_M=L$) and usually serves as a reference. For typical experimental conditions, this represents a small laser-beam width. This can be remedied by operating near the stability limit $g\to1$, which is the Fabry-Pérot geometry. However, such a cavity is very sensitive to misalignment and, as a compromise, one rather chooses to operate at $g\approx0.9$ or so. Another serious drawback of the spherical stable cavity is its multimode property. Indeed, besides the fundamental Gaussian mode, the higher-order Hermite-Gauss modes can also oscillate. This limits the quality of the output laser beam. In practice, modal selectivity is ensured by the use of small apertures. The fundamental mode is, however, also affected by this and its near-field pattern may show the familiar Fresnel ripples associated with hard-edged truncation.

Another way to increase the discrimination might consist in using *aspherical* mirrors. However, as mentioned above, in such a case the integral equation (2.1) cannot be solved analytically even in the limit $a\to\infty$. Bergstein and Schachter [15] have derived an approximate differential equation where the modal properties are described in terms of an equivalent potential related to the shape of the mirror. For the spherical mirror resonator, the potential is parabolic and their derivation is exact only for

this particular case. For any other profile, it seems impossible to assess *a priori* the error introduced by their approximation [see Eq. (8) of Ref. [15]] because it depends on the eigenmode itself. (Formally, it can be shown that this error vanishes for an infinitely long resonator, but this situation is not a practical one.)

The class of aspherical mirror resonator that we have recently introduced will be referred to here as "custom resonator" because the basic procedure for the design of the aspherical mirror starts with the specification by the users, of the intensity distribution on the output coupler. In this approach, the desired fundamental mode distribution is first propagated up to the mirror position; to limit the losses of this particular mode, the mirror is then made to conjugate this propagated field, i.e, that the mirror profile is chosen to correspond to the wave front of this mode at this position. In the limit $a \to \infty$, it has been shown [12] that the desired mode is indeed a solution of the integral equation. A numerical analysis is still necessary, however, if one wants to determine the higher-order modes and, hence, possibly improve the modal selectivity. It would thus be desirable to develop a theory that would give simple analytical information about the higher-order modes of this new class of resonators. This represents the aim of this paper. In the following we develop a perturbative analysis which shows that, asymptotically, the transverse modes obey a Schrödinger equation for which the potential-well corresponds to the mirror profile. In contrast with the work of Bergstein and Schachter [15], the limits of validity of the present model are clearly stated. Moreover, in Sec. III, the relevance of the approximations will be demonstrated for practical situations on the basis of numerical solutions of the exact problem (2.1).

B. Schrödinger differential equation for the transverse modes

Our model is based mainly on two approximations. First, we neglect edge diffraction ($a \to \infty$). This assumption is further discussed below. Second, because a wide fundamental mode is desirable, we consider a situation where the resonator length is much shorter than the diffraction length ("Rayleigh range") of this mode, i.e., $L \ll kw_0^2$. For instance, a spherical cavity with a resonator parameter $g \gtrsim 0.9$ is such that the dimensionless parameter d, defined as

$$d \equiv \frac{D}{2kw_0^2} , \tag{2.3}$$

is $\lesssim 0.06$ and can then be viewed as a perturbation parameter.

Bergstein and Schachter [15] based their analysis on the integral equation (2.1). However, they were unable to find a differential operator that would commute with the integral one. We then decided to attack the problem by instead using the paraxial wave equation

$$\frac{\partial^2 \psi}{\partial X^2} - i2k\frac{\partial \psi}{\partial Z} = 0 , \tag{2.4}$$

where ψ represents the slowly varying envelope of the electric field $U = \exp[-ikZ]\psi$ and Z corresponds to the propagation axis. To proceed, we now consider the equivalent half-symmetric resonator illustrated in Fig. 1(b), where the output coupler is a plane mirror [assuming unbounded mirrors, the mode on the coupler is then identical to the mode at the center of the symmetric cavity of Fig. 1(a)]. The eigenvalue problem (to be formulated as a differential eigenvalue equation) is now derived by following a mode for a complete round-trip. To allow a perturbative treatment, the paraxial wave equation is renormalized; the transverse dimension X is scaled as $x \equiv X/w_0$ and the longitudinal coordinate Z is expressed as $z \equiv Z/2kw_0^2$, so that the free-space propagation is now described by

$$\psi_{xx} - i\psi_z = 0 . \tag{2.5}$$

This equation can be formally integrated. In particular, the field Ψ' incident on the graded-phase mirror [Fig. 1(b)] is related to Ψ [$\equiv \psi(x, z=0)$] by

$$\begin{aligned} \Psi' &= \exp\left[-id\left[\frac{d^2}{dx^2}\right]\right]\Psi \\ &\equiv \mathcal{O}(d)\Psi , \end{aligned} \tag{2.6a}$$

where $\mathcal{O}(d)$ is the standard evolution operator in classical quantum mechanics [16]. This field is then reflected by the phase mirror to yield [Fig. 1(b)]

$$\Psi'' = \exp[i2\Phi]\Psi' . \tag{2.6b}$$

Similar to (2.6a), the return transit to the plane mirror is given by

$$\Psi''' = \mathcal{O}(d)\Psi'' . \tag{2.6c}$$

Finally, we close the loop by imposing the resonance condition

$$\Psi''' = \nu\Psi , \tag{2.6d}$$

where the eigenvalue ν is directly related to γ [Eq. (2.1)] when $a \to \infty$. The result of Eqs. (2.6) is an operatorial differential equation for the field distribution on the plane mirror [or, equivalently, at the center of the symmetric resonator of Fig. 1(a)] in terms of the mirror profile Φ:

$$\mathcal{O}(d)\exp[i2\Phi]\mathcal{O}(d)\Psi_n = \nu_n\Psi_n . \tag{2.7a}$$

We now restrict the analysis to the class of custom resonators described above. This means that the mirror profile Φ corresponds to the phase of the desired field distribution Ψ_0 propagated over the distance D, i.e., from (2.6a),

$$\Phi = \tan^{-1}\left[\frac{\left\{\sin\left[d\frac{d^2}{dx^2}\right]\right\}\Psi_0}{\left\{\cos\left[d\frac{d^2}{dx^2}\right]\right\}\Psi_0}\right] . \tag{2.7b}$$

The differential eigenvalue equation (2.7) is, in fact, a reformulation of the integral equation (2.1) in the limit $a \to \infty$. It contains the same information concerning the

modal properties of custom resonators. For an arbitrary resonator length, this certainly does not constitute an improvement over the original formulation. However, (2.7) has the serious advantage of allowing a simple perturbative approach in terms of the (here assumed) small parameter d. Indeed, Taylor expansions in d of the evolution operator (2.6a) and the mirror profile (2.7b) are then possible. In the following, we limit the expansion to $O(d^3)$. Then, from (2.7b) one finds

$$\Phi(x)=(V-E_0)d-\frac{1}{3}\left[\frac{1}{2}V_{xxxx}+2(V_x)^2+2(V-E_0)V_{xx}+2V_{xxx}\frac{\Psi_{0_x}}{\Psi_0}\right]d^3+O(d^5)\ , \quad (2.8)$$

where

$$V(x)\equiv\frac{\Psi_{0_{xx}}}{\Psi_0}+E_0\ . \quad (2.9)$$

Relation (2.9) is the stationary Schrödinger equation which univocally associates a potential $V(x)$ to the prescribed fundamental mode distribution Ψ_0. The constant E_0 is the corresponding energy level of the fundamental bound state (E_0 could be set to zero since the phase Φ is defined up to a constant. Here, it is chosen so that the eigenvalue ν_0 of the fundamental mode is purely real. In Sec. II C, this choice also implies that the stationary solutions of (2.9) have negative-energy levels).

The eigenvalue equation (2.7) is now solved using a regular perturbation method. The field Ψ and the eigenvalue ν are then expanded in powers of d:

$$\Psi=\Psi^{(0)}+d\Psi^{(1)}+d^2\Psi^{(2)}+\cdots\ , \quad (2.10)$$

$$\nu=\nu^{(0)}+d\nu^{(1)}+d^2\nu^{(2)}+\cdots\ . \quad (2.11)$$

From (2.7)–(2.11), one obtains, by identifying each term up to $O(d^3)$, the following.

For $O(1)$,

$$\nu^{(0)}=1\ . \quad (2.12)$$

For $O(d)$,

$$\Psi^{(0)}_{xx}+(E-V)\Psi^{(0)}=0\ , \quad (2.13)$$

$$\nu^{(1)}=i2(E-E_0)\ . \quad (2.14)$$

For $O(d^2)$,

$$\Psi^{(1)}=0\ , \quad (2.15)$$

$$\nu^{(2)}=-2(E-E_0)^2\ . \quad (2.16)$$

For $O(d^3)$ and for $V_{xx}\neq$const,

$$\Psi^{(2)}_{xx}+(E-V)\Psi^{(2)}+\tfrac{2}{3}V_{xx}(E-E_0)\Psi^{(0)}-\tfrac{2}{3}V_{xxx}\left[\Psi^{(0)}_x-\frac{\Psi^{(0)}_x}{\Psi^{(0)}_0}\Psi^{(0)}\right]=0\ , \quad (2.17)$$

$$\nu^{(3)}=-i\tfrac{4}{3}(E-E_0)^3\ , \quad (2.18)$$

and if $V_{xx}=C$(const),

$$\Psi^{(2)}_{xx}+(E-V)\Psi^{(2)}=0\ , \quad (2.19)$$

$$\nu^{(3)}=-i\tfrac{4}{3}(E-E_0)^3-i\tfrac{4}{3}C(E-E_0)\ . \quad (2.20)$$

The above equations represent the main result of this paper. Through Eq. (2.14), which identifies the energy level E to the eigenvalue ν, Eqs. (2.13)–(2.16) reveal a close relationship between the confined transverse modes of a custom resonator and the bound eigenstates of the stationary Schrödinger equation in quantum mechanics. Moreover, at this order, the associated potential corresponds exactly to the mirror profile. If the potential well $V(x)$ is sufficiently deep, it can support more than one bound state with energy levels $E_0,E_1,E_2,\ldots$, which implies that more than one confined mode could oscillate in the laser cavity. This equivalence was, of course, well known for the spherical resonator whose transverse modes, the Hermite-Gauss functions, are indeed the solutions of the corresponding harmonic oscillator. But it could only be conjectured for arbitrary mirror profiles. The now-established relationship is valid for $L\ll kw_0^2$ and applies to the *confined* modes of a stable custom resonator.

For higher-order corrections, one has to solve the nonhomegenous Schrödinger equation (2.17). The particular case of the fundamental mode is trivial; a comparison with Eq. (2.13) indicates that $\Psi_0^{(2)}=\Psi_0^{(0)}$, which is equivalent to setting $\Psi_0^{(2)}\equiv 0$ by a renormalization of $\Psi_0^{(0)}$. In physical terms, this means that the fundamental mode remains unchanged if the distance D between the mirrors is increased. This makes sense since by hypothesis, the graded-phase mirror is constructed from this mode; as defined above, the custom resonator is such that the fundamental mode is preserved whatever the length L is. The higher-order modes, however, will be modified (an example is given in Sec. II C). As suggested by Eqs. (2.19) and (2.20), the spherical resonator turns out to be an exception to this. Indeed, Eq. (2.19) indicates that, through a renormalization, *all the modes* remain unchanged at the next order. In fact, this particular case can be solved at any order with the correct conclusion that the Hermite-Gauss functions are indeed the transverse modes of the stable spherical cavity for any mirror separation. Equation (2.20) is then the third-order term of the expansion of the exact expression

$$\nu=\exp[i\sqrt{(2/C)}(E-E_0)\tan^{-1}(\sqrt{2C}d)]\ .$$

Similarly, for $V_{xx}\neq$const, (2.11) corresponds to the first terms of the expansion of $\exp[i2d(E-E_0)]$. In both cases, the confined modes are free of losses ($|\gamma|=1$), as can be expected for this conservative system.

C. A worked example: the Pöschl-Teller potential

The above analysis shows that by specifying the potential V or the fundamental mode Ψ_0, one can analytically predict the number of confined modes in the cavity as well as their field profiles. In contrast with the spherical case discussed above, one can now imagine a particular shape of mirror (potential) which would allow the oscillation of only a limited number of confined transverse modes. The interest of this is that in a practical situation

where the mirrors have a finite width, a mode which is not confined will lose more energy (in comparison with a confined mode) beyond the mirror edges at each round-trip in the cavity. Such a nonconfined mode is then highly discriminated in comparison with a confined one and this improves the quality of the output beam. As an example, here we consider the Pöschl-Teller potential [17,18]

$$v=-\mathcal{N}\operatorname{sech}^2 x \ , \tag{2.21}$$

where $\mathcal{N}$ is a positive number. We recall that, at first order in d, $V(x)$ also corresponds to the mirror profile [see Eq. (2.8)]. In a first analysis, we will present the modal solutions of (2.13) for $\mathcal{N}=2$ and 6 which predict 1 and 2 confined modes, respectively. The effects of higher-order terms $[O(d^3)]$ will be considered subsequently for the case $\mathcal{N}=6$. The results will confirm that the phase profile of all the confined modes do match the mirror profile.

For $\mathcal{N}=2$, the unique (unnormalized) bound mode of (2.13) is

$$\Psi_0^{(0)}=\operatorname{sech} x \ , \quad E_0=-1 \ . \tag{2.22}$$

Thus a laser cavity with a graded-phase mirror designed for this fundamental mode should support only this particular confined mode. This will be checked in Sec. III. In addition, (2.13) admits the following continuous spectrum of free eigenstates:

$$\Psi_\kappa^{(0)}=[\tanh x \mp i(\kappa-1)]\exp[\pm i(\kappa-1)x] \ , \tag{2.23}$$

$$E=(\kappa-1)^2 \ , \quad \kappa\geq 1 \ .$$

The case $\kappa=1$ ($\Psi_1^{(0)}=\tanh x$) corresponds to an energy level that is just at the limit of the potential well. To find the physical meaning of these solutions [Eq. (2.23)], one can notice that far off axis $\Psi_\kappa^{(0)}\sim\exp[\pm i(\kappa-1)x]$, i.e., that these free modes, in that region, correspond to uniform plane waves propagating back and forth in the cavity, making negative and positive angles with the Z axis. This makes sense because far from the axis the mirrors are essentially plane parallel and the resonator is then equivalent to a Fabry-Pérot geometry whose transverse modes (of the form $\cos x$ and $\sin x$, if hard-edged diffraction is neglected) can indeed be viewed as a superposition of such plane waves. In the present case, a linear combination of the free states (2.23) yields the following odd and even stationary modes (with a uniform wave front, as for the confined modes):

$$\Psi_{\text{odd}}^{(0)}=\tanh x\cos(\kappa-1)x+(\kappa-1)\sin(\kappa-1)x \ , \tag{2.24a}$$

$$\Psi_{\text{even}}^{(0)}=\tanh x\sin(\kappa-1)x-(\kappa-1)\cos(\kappa-1)x \ . \tag{2.24b}$$

In principle, κ is arbitrary (≥ 1) but, as for the Fabry-Pérot geometry, the boundary condition at the limit $X=a$ leads to a selection of discrete values for this parameter. As a crude (but sufficient for the purpose of this paper) approximation, one can impose the condition corresponding to a closed cavity, i.e., $\Psi(X=a)=0$ [19]. For the Fabry-Pérot geometry, this leads to the modes $\cos[m(\pi X/2a)]$ and $\sin[m(\pi X/2a)]$ with $m=1,2,\ldots$. Similarly, from (2.24), one obtains

$$\kappa_{\text{odd}}\approx 1+\frac{(2m+1)\dfrac{\pi}{2}}{\dfrac{a}{W_0}-1} \ , \tag{2.25a}$$

$$\kappa_{\text{even}}\approx 1+\frac{m\pi}{\dfrac{a}{W_0}-1} \tag{2.25b}$$

($m=0,1,2,\ldots$), where $a\gg W_0$ has been assumed. We must emphasize that the well-behaved functions (2.24) are only approximate expressions for the nonconfined modes when the mirrors are of finite width but edge diffraction is not taken into account. In fact, the closed-cavity approximation does not consider the unavoidable edge-wave diffraction which makes the actual modes severely rippled. This point will be further discussed in Sec. III.

For $\mathcal{N}=6$, there are two bound states, namely

$$\Psi_0^{(0)}=\operatorname{sech}^2 x \ , \quad E_0=-4 \ , \tag{2.26a}$$

$$\Psi_1^{(0)}=\operatorname{sech} x\tanh x \ , \quad E_1=-1 \ , \tag{2.26b}$$

together with the following continuous spectrum:

$$\Psi_\kappa^{(0)}=[3\tanh^2 x\mp 3i(\kappa-2)\tanh x-1-(\kappa-2)^2]\exp[\pm i(\kappa-2)x] \ , \tag{2.27}$$

$$E=(\kappa-2)^2 \ , \quad \kappa\geq 2 \ .$$

The existence of the second confined mode (2.26b) in a resonator adapted for the fundamental mode $\Psi_0=\operatorname{sech}^2 x$ will be verified in Sec. III. The free states (2.27) have the same physical interpretation as discussed above and can also be written in terms of odd and even real stationary modes.

Increasing the distance D between the mirrors will modify the modal distributions of the higher-order modes, as pointed out above. To describe this modification, one has to carry out the calculations to next order in d [Eqs. (2.17)–(2.20)]. Unfortunately, the analysis rapidly becomes cumbersome. Here, we present the results of an expansion to $O(d^3)$ for the second confined mode of the case $\mathcal{N}=6$. From Eq. (2.17), one finds the correction

$$\Psi_1^{(2)}=[\operatorname{sech} x\tanh x]S(x) \ , \tag{2.28a}$$

where

$$S(x)\equiv\sum_{n=1}^{\infty}c_n\tanh^{2n}x \ , \tag{2.28b}$$

$$c_1=-\frac{44}{3} \ , \quad c_n=-\frac{28}{15}\left[\frac{4n+6}{7n}\right] \quad (n=2,3,4,\ldots) \ ,$$

which can also be put in the closed form

$$S(x)=(c_1-\tfrac{6}{7}c_2)\tanh^2 x+\tfrac{4}{7}c_2\frac{\tanh^4 x}{\operatorname{sech}^2 x}-\tfrac{6}{7}c_2\ln(\operatorname{sech}^2 x) \ . \tag{2.28c}$$

This last equation indicates that $\Psi_1^{(2)}$ diverges at $x \to \pm\infty$, which means that the perturbation expansion of Ψ, at this order, is not uniform in x. Strictly speaking, the result (2.28) is only valid for sufficiently small values of x, i.e., close to the axis, to justify the expansion (2.10). This correction will be compared with a numerical example in Sec. III.

In contrast with the amplitude distribution, the perturbation expansion gives uniform results for the phase profile at $O(d^3)$. This is because higher-order terms in the series (2.28b) cancel out in (2.7b). For instance, propagation of Ψ_0 and Ψ_1 up to the mirror position gives, at $O(d^3)$, the respective phases Φ_0 and Φ_1 where the upper (lower) value corresponds to Φ_0 (Φ_1):

$$\Phi_{0,1} = d \begin{Bmatrix} 4-6\ \operatorname{sech}^2 x \\ 1-6\ \operatorname{sech}^2 x \end{Bmatrix} + d^3[32 - 472\tanh^2 x + 992\tanh^4 x - 552\tanh^6 x], \quad (2.29)$$

which, up to a constant factor, turn out to be the same. In physical terms, the wave front of each mode matches the mirror surface so that these modes are indeed conjugated [at least to order $O(d^3)$].

III. COMPARISON WITH NUMERICAL RESULTS

To demonstrate the interest of the reduction of the integral equation to a Schrödinger differential equation for the determination of the confined modes of an optical resonator, this integral equation [Eq. (2.1)] has been solved numerically using a Prony method [20]. In the following, we compare the predictions of our model with the exact modal properties of various symmetric resonators [Fig. 1(a)]: (i) a conventional spherical resonator providing a Gaussian fundamental mode $\Psi_0 = \exp[-(X/w_0)^2]$ at the center of the cavity, (ii) a custom resonator designed to yield $\Psi_0 = \operatorname{sech}[f_1 X/w_0]$, and (iii) another one for which $\Psi_0 = \operatorname{sech}^2[f_2 X/w_0]$. In order to make a fair comparison, scaling factors are introduced and adjusted so that the rms width of the fundamental mode is the same in the three cases ($f_1 = \pi/\sqrt{3} \cong 1.81$ and $f_2 = \sqrt{\pi^2/3 - 2} \cong 1.14$). The length L of the resonator is such that the geometric parameter of the spherical cavity g is equal to 0.9, a practical example. According to (2.2), the width w_0 of the Gaussian mode, at the center of the resonator, is then equal to $2.09 w_{\text{conf}}$ so that the parameter d is found equal to 0.057. This example should represent a good test of the usefulness of the present approximate model.

Figure 2(a) illustrates the exact phase profile of the three mirrors for a mirror width corresponding to a Fresnel number $N \equiv a^2/\lambda L = 10$. The vertical dashed lines refer to the width w_1 of the Gaussian mode on the spherical mirror [$w_0 \to w_1 = (1/\pi N)(1/1-g^2)^{1/2} a = 0.27a$]. This serves to indicate that the effective section of the mirror has roughly the same phase amplitude in the three cases. The higher selectivity of the sech^{1,2} resonators, expectable from their reduced number of confined modes and as demonstrated below, is largely due to the off-axis flattening of their mirror profiles. To get confident in the validity of the perturbative treatment, Fig. 2(b) compares the exact mirror profile of the sech^2 resonator (solid line) with the first-order term of the expansion (2.8) (i.e., an exact Pöschl-Teller potential) (dashed line). The agreement, which is already good, is further improved if the third-order term is also included, as indicated by the dotted line (almost indistinguishable from the exact profile).

Figure 3 shows the amplitude distribution of the first mode Ψ_0 of each resonator at the center of the symmetric cavity for $N = 10$. Because of the scaling factors f_i, these modes are very similar. At $N = 10$, the mirrors are wide enough to yield the expected Gaussian and sech^{1,2} distributions. The behavior is more interesting when one looks at the second mode (odd parity) Ψ_1 (Fig. 4). Whereas the spherical resonator nearly gives the $x \exp[-(x^2)]$ narrow distribution (solid line), the custom resonators provide substantially wider beams, particularly in the case of the sech^1 resonator (dashed line). This could be expected from the model developed in the preceding section. Indeed, this resonator is associated with a potential for which only one bound mode is possible. According to

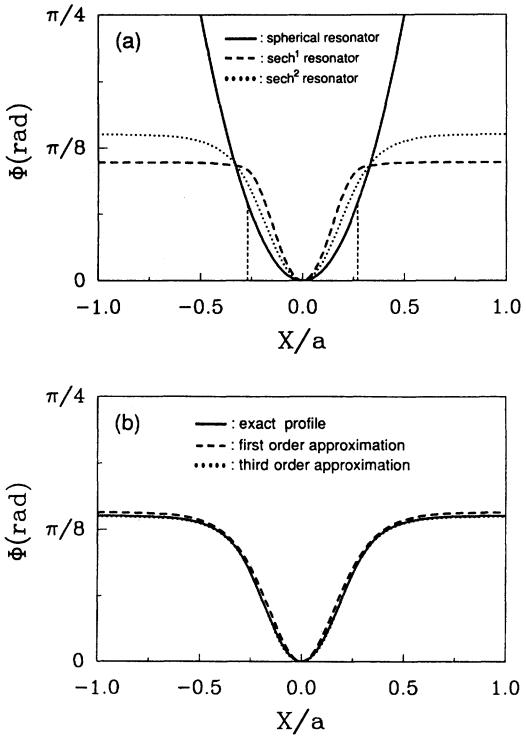

FIG. 2. (a) Exact mirror profile of the spherical resonator (solid line), the sech^1 resonator (dashed line) and the sech^2 resonator (dotted line). The X axis is normalized to the mirror radius. The vertical dashed lines represent the width of the Gaussian mode on the spherical mirror. $d = 0.057$ and $N = 10$. (b) Comparison between the exact mirror profile (solid line) of the sech^2 resonator and (i) its first-order approximation, i.e., the Pöschl-Teller potential (dashed line), (ii) its third-order approximation (dotted line).

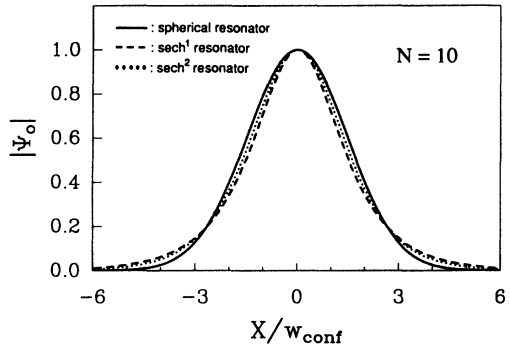

FIG. 3. Normalized amplitude profile of the fundamental mode at the center of the symmetric spherical resonator (solid line), the sech[1] resonator (dashed line) and the sech[2] resonator (dotted line) for $N=10$. The transverse coordinate X is normalized to the confocal spot size.

Eq. (2.23), the next eigenstate is $\Psi_1=\tanh(f_1x)$, which does not vanish at infinity [the approximation (2.24) is discussed below]. In the resonator, this mode would then be affected by edge diffraction and this explains the ripples observed in Fig. 4 (dashed line). This mode is not a confined mode and, as discussed in Sec. II C, round-trip power losses will discriminate against it in favor of the fundamental mode.

In contrast, the sech[2] resonator is expected to have two confined modes (as discussed in Sec. II), namely $\Psi_0=\text{sech}^2[f_2x]$ and $\Psi_1=\text{sech}[f_2x]\tanh[f_2x]$. Far off axis, the second mode decays as $\exp[-f_2x]$ and a wide mirror is then necessary in order to avoid edge diffraction and obtain the exact distribution. This is clearly demonstrated in Fig. 5 where Ψ_1 is shown for two different Fresnel numbers: $N=10$ [Fig. 5(a)] and $N=18$ [Fig. 5(b)]. The dashed line represents the $\text{sech}[f_2x]\tanh[f_2x]$ distribution. Figure 5(b) appears as a strong confirmation of the validity of the analogy with quantum mechanics. If the latter is correct, one could also predict that the third mode Ψ_2 of the sech[2] resonator, like the second mode of the sech[1] resonator, will be affected by the mirror edges. This is confirmed in Fig. 6 where the third mode of each resonator is presented ($N=10$). The strongly rippled pattern of this mode for the sech[1] and sech[2] resonators (dashed and dotted lines, respectively) is in sharp contrast with the well-confined third mode (nearly exact third Hermite-Gauss function) of the spherical resonator (solid line). To be further convinced of the absence of a third confined mode for the sech[2] resonator, the mirror width has been increased to $N=18$. In the conventional case [Fig. 7(a)], the confined

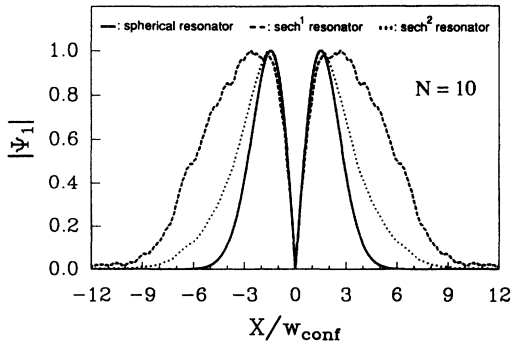

FIG. 4. Normalized amplitude profile of the second mode (odd parity) at the center of the symmetric spherical resonator (solid line), the sech[1] resonator (dashed line) and the sech[2] resonator (dotted line) for $N=10$. The transverse coordinate is normalized to the confocal spot size.

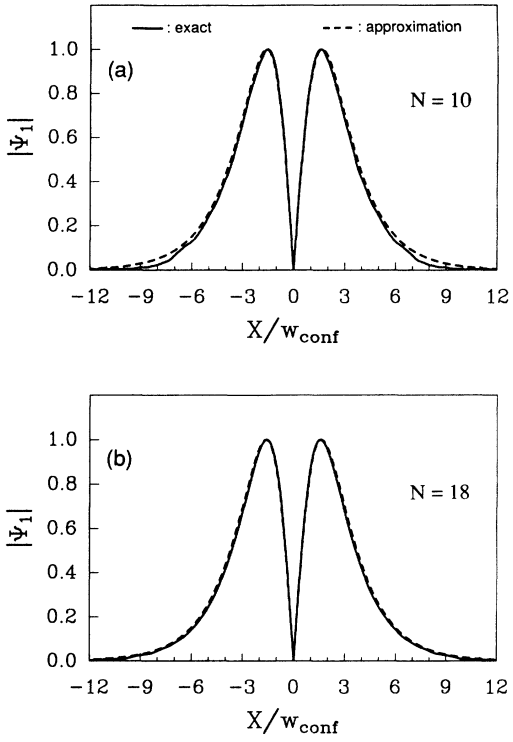

FIG. 5. Comparison between the exact amplitude distribution (solid line) of the second mode of the sech[2] resonator and the predicted $\text{sech}(f_2x)\tanh(f_2x)$ profile (dashed line) for (a) $N=10$ and (b) $N=18$.

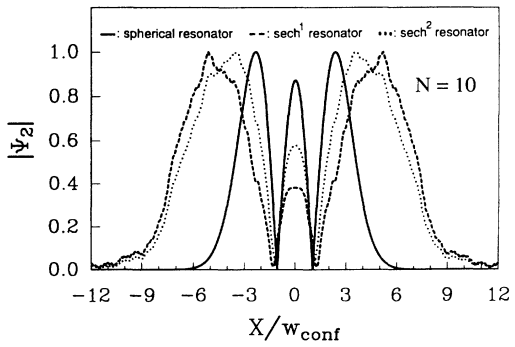

FIG. 6. Normalized amplitude profile of the third mode (even parity) at the center of the symmetric spherical resonator (solid line), the sech[1] resonator (dashed line), and the sech[2] resonator (dotted line) for $N=10$.

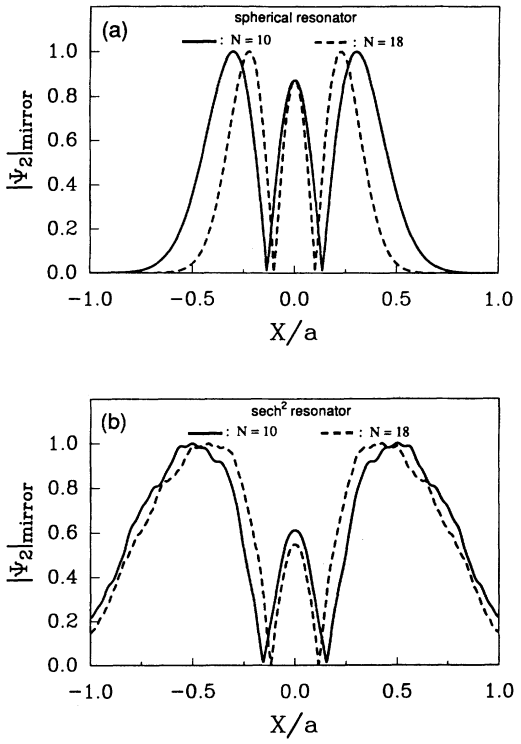

FIG. 7. Influence of the mirror width on the amplitude profile of the third mode on the mirror: (a) spherical resonator and (b) sech^2 resonator. Solid line, $N=10$; dashed line, $N=18$.

pattern on the mirror corresponding to $N=18$ (dashed line) is simply a scaled version of the previous one ($N=10$, solid line). This contrasts with the sech^2 resonator [Fig. 7(b)] where the amplitude at the edge of the mirror remains finite and the ripples persist simply because this mode is not confined.

The behavior of the higher-order modes means that the modal selectivity of these resonators should be quite different. This can be seen in Fig. 8 which shows the eigenvalue of the first eight modes as a function of the Fresnel number N ($1-|\gamma|^4$ represents the round-trip power losses). As expected, the behavior of the fundamental mode is quite similar in all cases; at $N \gtrsim 3$, this mode is practically lossless. Things are different for the other modes. Figure 8(a) shows the familiar multimodal property of the spherical resonator where all the higher-order modes also rapidly become nearly lossless as the Fresnel number is increased. This comes from the well-confined character of all these modes. This contrasts with the sech^2 resonator [Fig. 8(b)] where the existence of only two confined modes (as discussed above) is once more revealed. Modes which are not confined need a wide mirror before the energy lost beyond the mirror edges represents only a negligible fraction of their total energy. This is why the curves associated with these modes tend very slowly to the limit $|\gamma| \to 1$. Finally, the single-confined-mode characteristics of the sech^1 resonator is also confirmed in Fig. 8(c).

We now discuss the approximate expressions [Eqs. (2.24) and (2.25)] for the nonconfined modes of the sech^1 resonator. According to the discussion following Eq. (2.23), the second mode should not be compared with $\tanh(f_1 x)$ (which does not satisfy the closed-cavity boundary condition at $X=a$), but rather with the first odd approximation given by Eqs. (2.24a) and (2.25a) (with $m=0$; also $W_0 \to W_0/f_1$ and $x \to f_1 x$). This comparison is done in Fig. 9(a). Considering the simplicity of the derivation leading to this approximation, the agreement is surprisingly good. The third mode is also well approximated by Eqs. (2.24b) and (2.25b), as can be seen in Fig. 9(b). One can then conclude that the spreading of these nonconfined modes over all the mirror width is, in the average, well described by the approximate expressions (2.24). Before leaving this discussion, we must emphasize once more the essential distinction between a confined

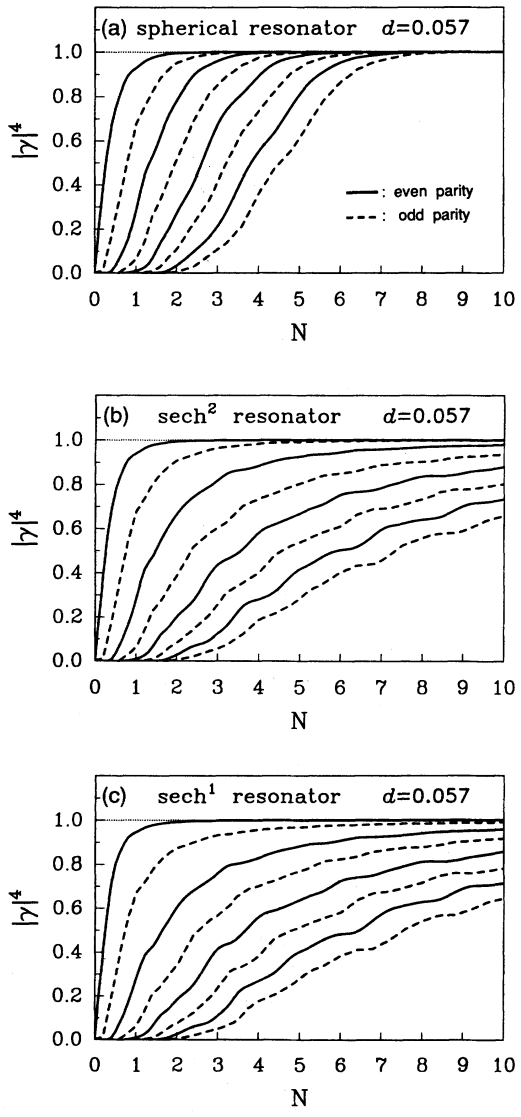

FIG. 8. Eigenvalue of the first eight modes as a function of the Fresnel number. Solid line, even parity; dashed line, odd parity. (a) spherical resonator; (b) sech^2 resonator; (c) sech^1 resonator. ($1-|\gamma|^4$) represents the round-trip power losses. Here $d=0.057$.

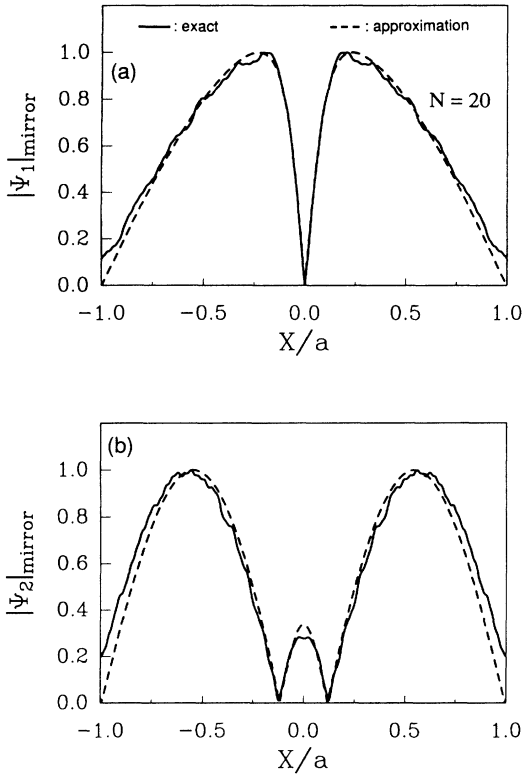

FIG. 9. Comparison between the exact amplitude distribution (solid line) of the nonconfined modes on the mirror of the sech[1] resonator and the approximation [Eqs. (2.24) and (2.25), dashed line] for $N=20$ and $d=0.057$. (a) Second mode; (b) third mode. The X axis is normalized to the mirror radius.

mode and a nonconfined one. As evidenced here, the latter is always affected by edge diffraction and is also discriminated in comparison with a confined mode.

Calculations for a sech[3] resonator have also been carried out (not shown here). They confirm the existence of three confined modes as can be predicted by the potential well model. The agreement on the amplitude profiles is also found to be as excellent as it is for the sech[2] resonator [Fig. 5(b)]. All these results demonstrate the relevance of the model and the validity of the underlying approximations.

The asymptotic approach has been shown to be justified for the most practical situation where the length of the cavity is relatively short in comparison with the Rayleigh range of the fundamental mode. For curiosity, we now consider a case where the geometric parameter is reduced to $g=0.5$, so that $w_0=1.32w_{conf}$ and $d=0.144$. As shown in Fig. 10, the behavior is qualitatively the same in what regards the modal selectivity. The amplitude distribution of the second mode of the sech[2] resonator is illustrated in Fig. 11 where it is compared with the first-order prediction, i.e., $\mathrm{sech}[f_2x]\tanh[f_2x]$ (dashed line). The agreement is not as good as it was before [Fig. 5(b)] and this is attributable to the relatively high value of the perturbation parameter d. In such circumstances, higher-order corrections must be included (see Sec. II). The dotted line in Fig. 11 corresponds to the third-order correction [Eq. (2.28)]. As discussed in Sec. II, the correction strictly applies near the axis where indeed, as can be seen in Fig. 11(b), it does improve the approximation. It also correctly predicts the "shrinking" of the mode here observed.

On the basis of these results, one might be tempted to extrapolate and conclude that the sech[1,2] resonators remain highly selective for any mirror separation. However, counter examples can be given. For instance, we have observed that the mirror profile of a sech[1] resonator becomes almost perfectly parabolic (over a wide transverse extent) at some particular finite distances so that, in practice, in those cases the cavity would become multimodal.

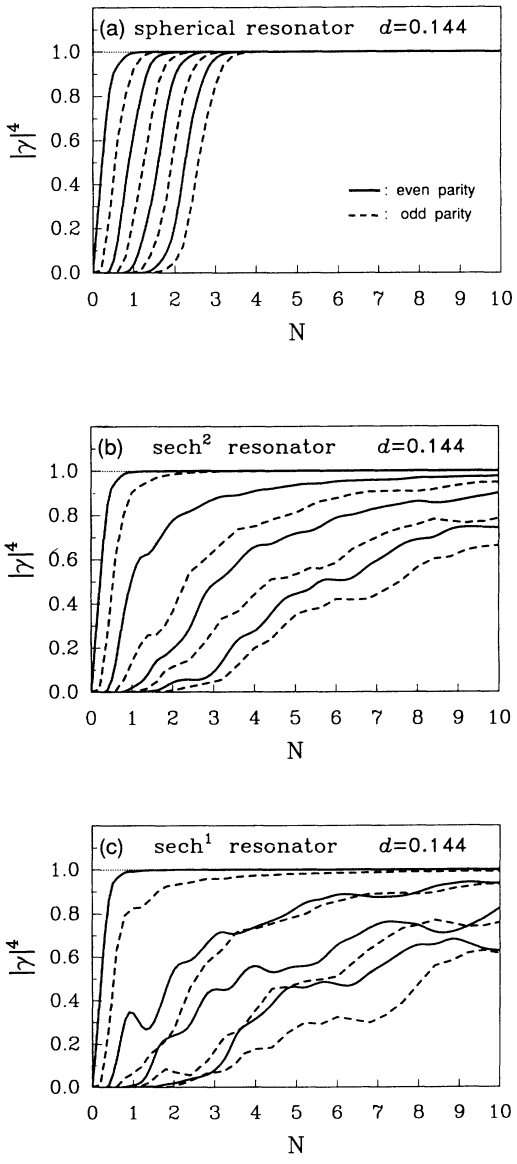

FIG. 10. Same as Fig. 8, except that the resonator length is increased to $d=0.144$.

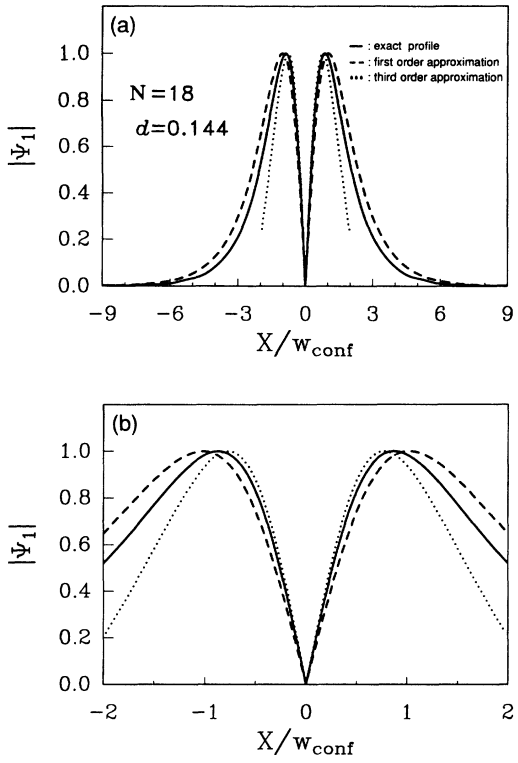

FIG. 11. (a) Comparison between the exact amplitude distribution (solid line) of the second mode of the sech^2 resonator and (i) the first-order prediction $\mathrm{sech}(f_2x)\tanh(f_2x)$ (dashed line); (ii) the third-order prediction (dotted line) for $N=18$ and a resonator length increased to $d=0.144$. (b) An enlargement of the central region.

IV. CONCLUSION

In this paper, for simplicity, we have considered a one-dimensional geometry. The analytical tractability of the Pöschl-Teller potential may then serve to demonstrate the interest of the model. Besides this pedagogical advantage, the strip geometry may also correspond to practical laser systems. This is the case, for instance, when a slab gain medium is used for the amplification, a configuration for which there is now a growing interest. Obviously, the analogy with quantum mechanics can be extended to the circular geometry. The azimuthal degree of freedom may increase the difficulty (in the sense of reduced analytical possibilities), but the main physical properties should be preserved.

For the most practical situation where the length of a resonator can be considered as being short in comparison with the Rayleigh range of the fundamental mode, it has been shown that the transverse modes of a custom resonator are directly linked to the eigenstates of the stationary Schrödinger equation with a potential corresponding to the mirror profile. The demonstration relies on a powerful approach based on the paraxial wave equation rather than the Huygens-Fresnel integral which makes possible the formulation of the eigenvalue problem as a differential eigenvalue equation. Then, a perturbation method based on Taylor expansions of the evolution operator and the mirror profile leads to the analogy with quantum mechanics. This method has the benefit of clearly stating the limits of validity of the equivalence and it allows the explicit evaluation of higher-order corrections when a longer cavity is considered.

We believe that the same approach can be easily applied to other systems. In particular, we are presently investigating the possible advantages of adding a graded reflectivity as a way to increase the modal selectivity. The analysis of the influence of a misalignment is also under progress. Similarly, the present work could be extended by including a gain and/or a nonlinear medium in the cavity. But, as it stands, the present model already represents a valuable tool for designing custom resonators whose higher-order modes would be either nonconfined or much wider than the fundamental mode so that they could be easily eliminated by using finite apertures. In that sense, we have reached the objective we had in mind at the beginning of this work which consisted in getting simple analytical information on the nature of the higher-order modes of a custom resonator.

ACKNOWLEDGMENTS

This research was supported by the Fonds pour la Formation de Chercheurs et l'Aide à la Recherche FCAR of the Gouvernement du Québec and the Natural Science and Engineering Research Council (NSERC) of the Government of Canada.

*FAX: (418)-656-2623.

[1] A. E. Siegman, *Lasers* (University Science Books, Mills Valley, CA, 1986), Chap. 19.
[2] Yu. A. Anan'ev, *Résonateurs Optiques et Problème de Divergence du Ravonnement Laser* (Editions Mir, Moscow, 1982), Chap. 2.
[3] A. Yariv, *Quantum Electronics,* 3rd ed. (Wiley, New York, 1989), Chap. 7.
[4] See, for example, Ref. [1], Chap. 12; Ref. [2], Chap. 1; and Ref. [3], Chap. 9.
[5] See, for example, Ref. [1], Chap. 23; and Ref. [2], Chap. 2, and references therein.
[6] See, for example, Ref. [1], Chap. 23, and references therein.
[7] E. F Ishchenko and E. F. Reshetin, Opt. Spektrosk. **51**, 1050 (1981) [Opt. Spectrosc. (USSR) **51**, 581 (1981)].
[8] M. Lax, C. E. Greninger, W. H. Louisell, and W. B. McKnight, J. Opt. Soc. Am. **65**, 642 (1975).
[9] See also, Ref. [2], Chap. 2, and references therein.
[10] T. R. Ferguson and M. E. Smithers, J. Opt. Soc. Am. A **1**, 653 (1984), and references therein.
[11] P.-A. Bélanger and C. Paré, Opt. Lett. **16**, 1057 (1991).
[12] C. Paré and P.-A. Bélanger, IEEE J. Quantum Electron. **QE-28**, 355 (1992).
[13] P. A. Bélanger, R. L. Lachance, and C. Paré, Opt. Lett. **17**, 739 (1992).

[14] See, for example, Ref. [1], Chap. 19.
[15] L. Bergstein and H. Schachter, in *Proceedings of the Symposium on Modern Optics,* edited by J. Fox (Polytechnic, Brooklyn, 1967), Vol. XVII, p. 527.
[16] C. Cohen-Tannoudji, B. Diu, and F. Laloë, *Mécanique Quantique* (Hermann, Paris, 1977), Tome I, Chap. 3.
[17] G. Pöschl and E. Teller, Z. Phys. **83**, 143 (1933).
[18] P. M. Morse and H. Feshback, *Methods of Theoretical Physics* (McGraw-Hill, New York, 1953), Tome II, p. 1650.
[19] For a deeper analysis of the Fabry-Pérot geometry see, L. A. Vainshtein Zh. Eksp. Teor. Fiz. **44**, 1050 (1963) [Sov. Phys.—JETP **17**, 709 (1963)]; see also, P. A. Bélanger and A. Légaré, Can. J. Phys. **52**, 1981 (1974).
[20] For a detailed description of this method, see A. E. Siegman and H. Y. Miller, Appl. Opt. **9**, 2729 (1970).